Biosensors and Bioelectronics 142 (2019) 111509

Contents lists available at ScienceDirect

Biosensors and Bioelectronics

journal homepage: www.elsevier.com/locate/bios

Dual-function nanostructured platform for isolation of nasopharyngeal carcinoma circulating tumor cells and EBV DNA detection

Sheng-Wei Lee[a,b,1], Yi-Wei Chen[a,1], Edward C. Kuan[c], Ming-Ying Lan[d,e,*]

[a] Institute of Materials Science and Engineering, National Central University, Taoyuan City 32001, Taiwan
[b] Department of Materials Science and Engineering, University of California, Irvine, Orange, CA 92697, USA
[c] Department of Otolaryngology-Head and Neck Surgery, University of California, Irvine, Orange, CA 92868, USA
[d] Division of Rhinology, Department of Otolaryngology Head and Neck Surgery, Taipei Veterans General Hospital, Taipei, 11217, Taiwan
[e] School of Medicine, National Yang-Ming University, Taipei, 11221, Taiwan

ARTICLE INFO

Keywords:
Nasopharyngeal carcinoma
Circulating tumor cells
Si
Nanowire
EBV DNA
EpCAM

ABSTRACT

Circulating tumor cells (CTCs) and plasma levels of Epstein–Barr virus (EBV) DNA are sensitive prognostic tools for monitoring disease status in nasopharyngeal carcinoma (NPC) patients. Herein, we introduce a novel and low-cost platform for capturing CTCs, the Si nanowires/microscale pyramids (NWs/MPs) hierarchical substrate, which could capture NPC cells in vitro and also detect EBV DNA at very low concentrations. In this study, Si NWs/MPs hierarchical substrates with varying wire length were fabricated using a metal-assisted chemical etching method. Anti-EpCAM antibodies were further conjugated on the substrate for capturing NPC CTCs in vitro. Capture efficiency was evaluated using immunofluorescence and scanning electronic microscopy (SEM) was utilized to understand cell morphology. The Si NWs/MPs substrate was also transformed into a Surface enhanced Raman scattering (SERS) substrate by coating with Ag nanoparticles (AgNPs) for detection of EBV DNA by Raman spectroscopy. The results demonstrated that Si NWs/MPs with 20 min of etch time had the best capturing performance. Additionally, SEM observations revealed good contact of CTCs with Si NWs/MPs substrates. Moreover, the AgNPs-coated NWs/MPs substrate was shown to be a sensitive EBV DNA detector, by which the DNA detection limit can reach up to 10^{-13}M. In conclusion, the Si NWs/MPs platform not only exhibits superior cell capturing ability, but also can sensitively detect EBV DNA at very low concentrations. This platform has great potential to become a promising diagnostic tool for monitoring disease status and prognostication of NPC patients.

1. Introduction

Nasopharyngeal carcinoma (NPC) is a unique epithelial malignancy arising from nasopharyngeal mucosa. It is a common cancer in southern China and southeast Asia, but relatively rarer in western countries (Chua et al., 2016; Petersson, 2015). NPC has been proposed to result from a multifactorial etiologies, including genetic susceptibility, EBV infection, and environmental factors, such as consumption of salted foods. The pathogenesis of NPC is thought to be a complex interaction between viral infection and multiple somatic genetic and epigenetic changes, which synergistically disrupt normal cell function (Bruce et al., 2015; Petersson, 2015). Most NPC cases are of the non-keratinizing subtype, associated with Epstein–Barr virus (EBV), and tend to be highly responsive to radiotherapy. Despite a good response to treatment in the majority of case, some patients still experience local recurrence or distant metastases even after receiving precise radiotherapy as well as chemotherapy, which accounts of significant morbidity and mortality. Therefore, discovering useful tools for early detection of tumor recurrence and distant metastasis is highly important.

Modern cancer research has demonstrated that the presence of circulating tumor cells (CTCs) play a critical role in the process of metastasis (Fidler, 2003). Detection of CTCs is analogous to “liquid biopsy”, which is a noninvasive and easily repeatable technique. This process not only reveals active metastasis, but also helps to monitor disease progression by providing real-time information about the patient's disease status (Attard et al., 2009; Schlange and Pantel, 2016). It is proposed that CTCs may be of help to facilitate and determine appropriate tailored treatments for patients. Presently, several methods have been developed to isolate and enumerate CTCs (Paterlini-Brechot and Benali, 2007), and these techniques has been used for detecting

* Corresponding author. Department of Otolaryngology, Taipei Veterans General Hospital, No.201, Sec. 2, Shipai Rd, Beitou District, Taipei, Taiwan 11217
E-mail addresses: swlee@g.ncu.edu.tw (S.-W. Lee), eckuan@hs.uci.edu (E.C. Kuan), mylan@vghtpe.gov.tw (M.-Y. Lan).
[1] The first 2 authors contributed equally to this article.

https://doi.org/10.1016/j.bios.2019.111509
Received 5 May 2019; Received in revised form 11 July 2019; Accepted 12 July 2019
Available online 18 July 2019
0956-5663/

CTCs in various epithelial cancers (Danila et al., 2011; Miller et al., 2010; Swaby and Cristofanilli, 2011; Zhe et al., 2011). The presence of CTCs has been shown to be a valuable and strong prognosticator for overall survival in patients with metastatic breast, colorectal, prostate, and non-small cell lung cancers (Cohen et al., 2008; Doyen et al., 2012; Farace et al., 2011; Krebs et al., 2011).

Although there is mounting evidence reporting the detection of CTCs in various cancers, there are currently limited studies on application of CTCs in NPC (Chen et al., 2018; Li et al., 2016; Wu et al., 2017). Among these studies, distinct detection methods were used, including the magnetic bead isolation technique and Isolation by Size of Epithelial Tumor (ISET) method (Chen et al., 2018; He et al., 2017; Li et al., 2016; Wu et al., 2017). CTCs were identified as nuclear cells without CD45 expression, and some studies have combined CK18 with the FISH-centromere of chromosome 8 (CEP8) probe (Chen et al., 2018). Previous work in our lab had successfully utilized nanotechnology to develop optimal titanium oxide (TiO_2) nanofibers coated with anti-epithelial-cell adhesion-molecule (anti-EpCAM) antibodies for capturing NPC cells in vitro (Zeng et al., 2017). In this study, we further designed and fabricated a more cost-effective platform, Si nanowires/microscale pyramids (NWs/MPs) hierarchical substrates, which not only effectively captures CTCs, but also detects EBV DNA with high degree of sensitivity.

2. Materials and methods

2.1. Cell culture

NPC cell lines (TW01) provided by Dr. C.T. Lin (National Taiwan University, Taiwan) were derived from primary nasopharyngeal tumors of Chinese patients with *de novo* NPC and had been previously tested and authenticated (Lin et al., 1990, 1993). NPC cell lines were maintained in DMEM with 10% FBS containing penicillin (100 U/mL) and streptomycin (100 μg/ml) in 5% CO_2 at 37 °C. U937 (monocytes) were purchased from Bioresource Collection and Research Center (BCRC) (No. 60435). U937 cells were maintained in RPMI 1640 medium containing 2 mM L-glutamine adjusted to contain 1.5 g/L sodium bicarbonate, 4.5 g/L glucose, 10 mM HEPES, 1.0 mM sodium pyruvate, and 10% fetal bovine serum.

2.2. Fabrication of Si NWs/MPs hierarchical structures

A (100) oriented Si wafer (Boron-doped 1–10 Ω cm) was ultrasonically cleaned in acetone, isopropanol, and ethanol each for 5 min to remove contaminants. The cleaned Si wafer was then etched in solution containing 600 ml DI-water, 55 ml potassium hydroxide (KOH), and 45 ml isopropanol for 1 h at 82 °C to produce micrometric pyramids on the Si substrate. Then, the NWs/MPs hierarchical structures were fabricated by a two-step metal-assisted chemical etching method. The first step was to dip the Si pyramid substrate into the solution of 78 ml DI-water, 22 ml hydrofluoric acid (HF), and 2 ml 0.1 N silver nitrate ($AgNO_3$) at 25 °C for 30 s, depositing Ag nanoclusters on the surface of pyramid substrate. The pyramid substrate is then etched in a solution of 78 ml DI-water, 22 ml HF, and 6.8 g $Fe(NO_3)_3.9H_2O$ for 10, 20, 30, 40 min to produce the so-called Si NWs/MPs hierarchical structure with different wire lengths. The residual Ag clusters on the surface were then removed by the ultrasonic vibration.

For EBV DNA detection, the Si NWs/MPs substrates were further dipped in the 0.002 M $AgNO_3$ for 1 min to fabricate the AgNPs-coated NWs/MPs.

2.3. Surface modification of Si NWs/MPs

The surface of the Si NWs/MPs substrate was first modified with 4% (v/v) 3-mercaptopropyl trimethoxysilane (MPTMS) in absolute ethanol by silane chemistry for 1 h. Then, 0.25 mM N-maleimidobutyryloxy succinimide ester (GMBS) in DMSO solution was added as a coupling agent for 1 h, followed by 10 μg ml/L of streptavidin (SA) for 30 min at 25 °C. There are two reactive groups in the GMBS molecule, maleimide and N-hydroxysuccinimide, which are reactive towards the sulfhydryl group in MPTMS and amino group in SA, respectively. After excess SA was removed with PBS, the modified substrate was dipped into biotinylated antinylated anti-EpCAM (2 μg/ml in PBS, goat anti-human EpCAM polylclonal antibody, R & D System, Inc., USA) for 30 min for anti-EpCAM conjugation.

2.4. Cell capture and detection

The substrate was placed into a chamber of 12-well culture plate and 1 ml cell suspensions (10^3 cells/mL, EpCAM-positive NPC TW01 cell line) was incubated for 1 h. The substrate was then gently rinsed with PBS at least 5 times. The captured cells were fixed in 4% paraformaldehyde for 20 min at room temperature and washed with PBS. After fixation, the cells were permeabilized with 0.2% Triton X-100 in PBS for 10 min at 4 °C. Cells were then washed with PBS and incubated in diamidino-2-phenylindole (DAPI; Thermo Fisher Scientific Inc., Waltham, MA, USA) for 5 min for nucleic staining. Fluorescent microscopy (AX80, Olympus) was used to image and count the substrate-immobilized cells. Capture efficiency of different Si NWs/MPs hybrid structure was calculated using ImageJ software (U.S. National Institutes of Health,http://rsb.info.nih.gov/ij/download.html). U937 cells were used as the negative control.

2.5. Immunofluorescence study

The substrate was submerged in 1 ml NPC cell suspensions (10^3 cells/mL) in a chamber of 12-well culture plate and incubated for 1 h. The substrate was then gently rinsed with PBS at least 5 times. The captured cells were fixed in 4% paraformaldehyde for 20 min at room temperature and washed with PBS. After fixation, the cells were permeabilized with 0.2% Triton X-100 in PBS for 10 min at 4 °C. Cells were then blocked with 5% BSA for 30 min, followed by incubation using a cocktail of primary antibodies: mouse anti-human vimentin monoclonal antibody (1:350, GTX629744, GeneTex, Inc., USA) and rabbit anti-human cytokeratin 8 + 18 monoclonal antibody (1:350, ab53280, Abcam, USA), or mouse anti-human CD45 monoclonal antibody (1:350, GTX628507, GeneTex, Inc., USA) alone at room temperature for 1 h. For visualization, a cocktail of secondary antibodies were used at a concentration of 2 μg/mL in PBS at room temperature for 45 min: donkey anti-mouse conjugated to Alexa Fluor 555 and donkey anti-goat conjugated to Alexa Fluor 488, or donkey anti-rabbit conjugated to Alexa Fluor 555 and donkey anti-mouse antibodies conjugated to Alexa Fluor 488 (Invitrogen Corp., Carlsbad, CA). DAPI (Thermo Fisher Scientific Inc., Waltham, MA, USA) was used for nuclei stain for 5 min. Images were then acquired under a fluorescent microscope (AX80, Olympus).

To investigate the sensitivity and specificity of the substrate regarding capturing cells, NPC TW01 cells were pre-stained with CFSE solution (CFSE Cell Division Tracker kit, BioLegend, San Diego) at 37 °C for 20 min, while U937 cells were pre-stained with Hoechst solution (Thermo Fisher Scientific, USA) at 37 °C for 15 min. The substrate was then cultured with a mixture of 1×10^2 NPC TW01 cells (green, fluorescence) and 1×10^2 of U937 cells (blue fluorescence) in a final volume of 50 μL. The captured cells on the substrate and the cells in supernatant (both NPC cells and U937 cells) were counted under a fluorescent microscope (AX80, Olympus) to calculate the sensitivity and the specificity of the substrate.

2.6. Scanning electronic microscopy (SEM)

The morphology of the captured cells and the microstructure of the substrates were examined by SEM (FEI Quanta 200F). Before SEM

observation of the captured cell, the cells were first treated with 2.5% glutaraldehyde solution (Merck) for 1 h. Then the cells were dehydrated through serial gradients with mixtures of ethanol and distilled water (40, 50, 60, 70, 80, 90, and 100%) and dried with a Critical Point Dryer (CPD 030, Leica). Last, thin gold was coated on the cells for SEM observations.

2.7. Preparation of Ag NPs modified with 4-MBA and EBV target DNA

AgNPs modified with 4-MBA and EBV target DNA were prepared for analysis (Lin et al., 2015; Zhang et al., 2012b). Briefly, 6 μl of DNA stock solution (1 μM) was added into 1 ml of 60 nm AgNPs (1 nM) and mixed by a brief vortexing, to yield a final 500 μl EBV target DNA solution. 5 μl of 500 mM pH 3 citrate buffer was then added into the AgNPs solution and vortexed briefly, followed by incubation at room temperature for 5 min. The same amount of the pH 3 buffer solution was added into the DNA-AgNPs mixture again to achieve a final pH 3 10 mM buffer. After incubation at room temperature for 25 min for DNA loading, 15 μl of 500 mM pH 7.6 HEPES buffer was added to adjust the pH of the AgNP solution to neutral pH. The DNA-AgNPs mixture was then centrifuged for 30 min at 13000 rpm. The supernatant was removed, and the pellet was washed 2–3 times with 5 mM HEPES, followed by centrifugation to remove free DNA completely. The washed DNA-AgNPs conjugate was re-dispersed in 5 mM HEPES buffer (pH7.6) for further use.

1 ml of aqueous dispersion of AgNPs modified with the EBV target DNA was then mixed with 0.5 ml of 4-MBA ethanol solution (0.1 M) for 20 min. After 30 min of centrifugation (13000 rpm), the pellet comprising 4-MBA functionalized AgNPs was washed with ddH2O using centrifugation to get rid of unbound 4-MBA molecules. Finally, 4-MBA functionalized DNA-AgNPs conjugate were re-dispersed in 1X PBS.

2.8. Hybridization procedures and surface-enhanced Raman spectroscopy (SERS) experiments

First, 0.5 ml of the EBV probe DNA (1 μM) was added on the AgNPs-coated substrates and incubated for 2 h at room temperature with shaking. Afterwards, the sheets were washed 3 times with 1X PBS to remove unbound probe DNA, and then treated with 0.5 ml silver nanoparticles modified with 4-MBA and EBV target DNA for another 2 h at room temperature with shaking. The substrates were then thoroughly washed and immersed in ddH2O for 1 h. Finally, the substrates were air-dried. The SERS spectra of 4-MBA were collected using a Micro-Raman spectroscopic system (PTT-EL) with 532 nm excitation laser. The Raman spectra integration time was 20 s for each location. Signals at 1078 and 1596 cm-1 indicate hybridization of target EBV DNA and probe DNA.

2.9. Statistical analysis

All experiments were carried out in triplicate and at least three independent experiments were performed. Data were presented as mean ± standard error (SE) and analyzed by analysis of variances (ANOVA) using SPSS 12.0 software (SPSS Inc.). A p value of < 0.05 was considered statistically significant.

3. Results

3.1. Characterization of the Si NWs/MPs substrate

Herein, we fabricated a novel and cost-effective platform for capturing CTCs, the Si NWs/MPs hierarchical substrate (as shown in Fig. 1), in which the nanowire length was precisely controlled by subjecting different etching times. The nanowire lengths of 1.5 μm, 3.8 μm, 5.1 μm and 6.9 μm were produced after the metal-assisted chemical etching for 10 min, 20 min, 30 min and 40 min, respectively. Therefore, a series of Si NWs/MPs substrates with NW lengths varying from 1.5 to 6.9 μm were obtained. Fig. 2A shows the SEM tilt views and cross views of various Si NWs/MPs substrates (First row: 3000X, Second row: 10000X). The crater on the top of the pyramid became larger and the surface morphology also became smoother simultaneously when the substrate received longer exposure time. In addition, due to the denser charge distribution and the faster mass transport in the etching process, the etching rate at the tip of pyramids was significantly faster than other area. The denser charge distribution at the tip of pyramids resulted from the difference in electronegativity between the Si substrate and AgNPs reduced form $AgNO_3$ around the tips of pyramids.

3.2. Quantitative detection of NPC CTCs

After fabricating the Si NWs/MPs substrate, we functionalized the substrate with MPTMS and GMBS, followed by adding SA and then conjugated with anti-EpCAM antibodies (Fig. 1). To test the cell-capture performance of the Si NWs/MPs substrates, a cell suspension (10^3 cells/mL) of an EpCAM-positive NPC cell line (i.e., TW01) in cell culture medium (DMEM) was introduced onto the Si NWs/MPs substrate for 1 h.

Fig. 3A demonstrates the results of the various substrates to capture CTCs (NPC TW01), and the mean counts of both the NPC TW01 cells as well as the negative control cells (U937) was shown in bar chart in Fig. 3B. Captured cells were stained with DAPI. In this study, U937 cells were used as a negative control since they were lacking EpCAM expression. Therefore, U937 cells barely captured by the substrates coated with Anti-EpCAM antibodies (Supplementary Fig.1). The probability of capturing CTCs should be proportional to the concentration of antibodies coated on the substrate, which should be related to the surface area of the substrate. Therefore, plain silicon and pyramid substrates had the lowest amount of captured CTCs because of their relative lesser surface area. Among various Si NWs/MPs structures, the 20 min-etched design captured significantly more CTCs than the others. There was no significant difference of capture ability between 10 min-, 30 min- and 40 min-etched Si NWs/MPs structures. We further conducted immunofluorescence studies and demonstrated that most captured cells were positive for EpCAM, vimentin, CK 8 + 18, while negative for CD45 (Supplementary Fig. 2). The CTC capture efficiency of the best platform (20 min-etched Si NWs/MPs) was 84.5 ± 1.19%; specificity was 74 ± 2.68% and sensitivity was 78.25 ± 5.19% (Supplementary Fig. 3).

3.3. Cell contact between CTCs and Si NWs/MPs substrate

The SEM images of CTCs adhering to different substrates are shown in Fig. 4A. Both lamellipodia and filopodia could be observed on the edge of the NPC cells on various substrates. Compared to CTCs on plane substrates, CTCs on Si NWs/MPs seems to have wider surface areas of spread which promote cell contact with the substrate, leading to relatively more lamellipodia being observed (Fig. 4A). The filopodia of CTCs on Si NWs/MPs were also dispersed vertically down into the gaps between the nanowires which may further increase cell adhesion (Fig. 4B).

3.4. Quantitative detection of EBV DNA

We further prepared the AgNPs-coated etched or unetched plane and NWs/MPs to test for capturing EBV DNA (Fig. 2B). Fig. 2B shows the SEM views of different substrates coated with AgNPs. Fig. 5 is the schematic illustration of EBV DNA captured on Si NWs/MPs coated with AgNPs. Fig. 6 show the SERS results of EBV DNA detection by using the various AgNPs-coated substrates. Higher EBV DNA concentration led to higher laser-scattering intensity, indicating higher amounts of captured EBV DNA. The AgNPs-coated NWs/MPs substrate captured the greatest amount of EBV DNA, followed by the AgNPs-

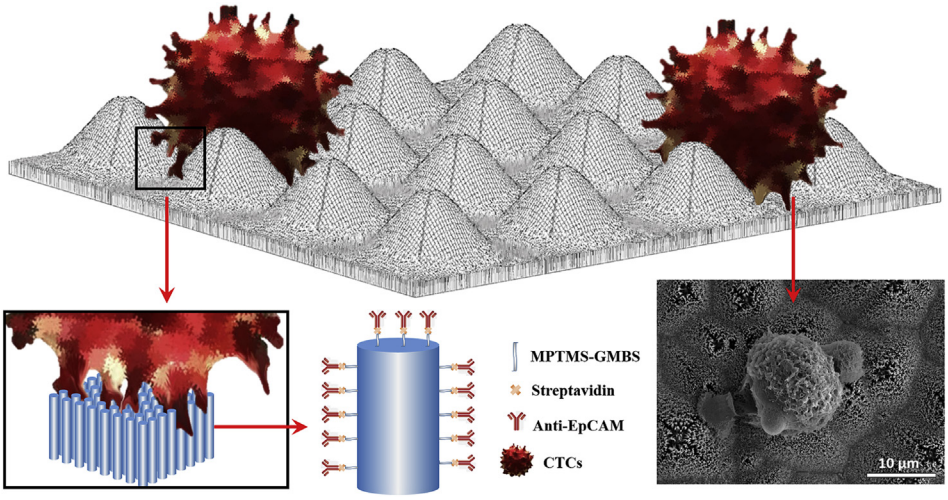

Fig. 1. Schematic illustration of CTCs captured on the Si NWs/MPs substrate. The Si NWs/MPs substrate was functionalized with MPTMS and GMBS, followed by adding SA and then conjugated with anti-EpCAM antibodies before capturing CTCs.

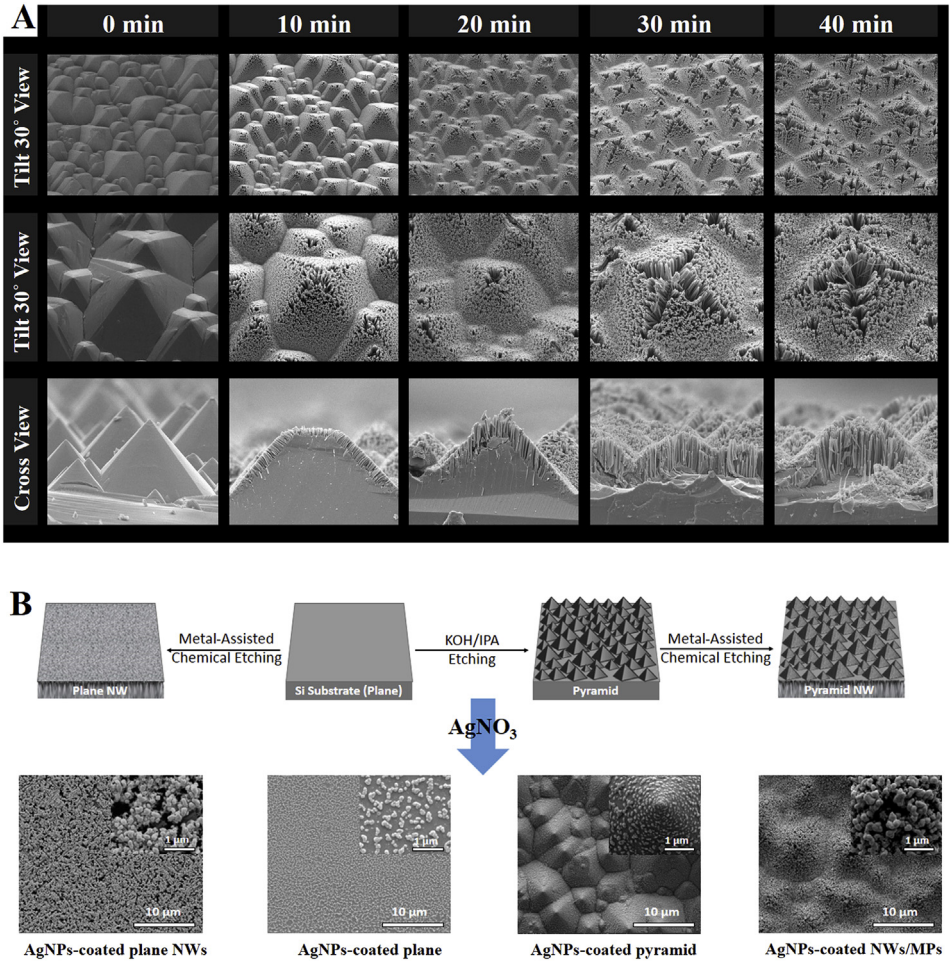

Fig. 2. (A) The SEM views of various Si NWs/MPs substrates. The nanowire lengths of 1.5 μm, 3.8 μm, 5.1 μm and 6.9 μm were produced after the metal-assisted chemical etching for 10 min, 20 min, 30 min and 40 min, respectively. (First row: SEM tilt views of the NWs/MPs, 3000X. Second row: SEM tilt views of the NWs/MPs, 10000X. Third row: SEM cross views of the NWs/MPs, 12000X.) **(B) Schematic illustration of fabrication of AgNPs-coated plane, NWs, pyramid, and NWs/MPs.**

coated plane NW, AgNPs-coated pyramid, and AgNPs-coated plane substrates (Fig. 6E) (Supplementary Fig. 6). Moreover, the AgNPs-coated NWs/MPs substrate was shown to be a sensitive EBV DNA detector, by which the DNA detection limit can reach up to 10^{-13}M (Fig. 6D).

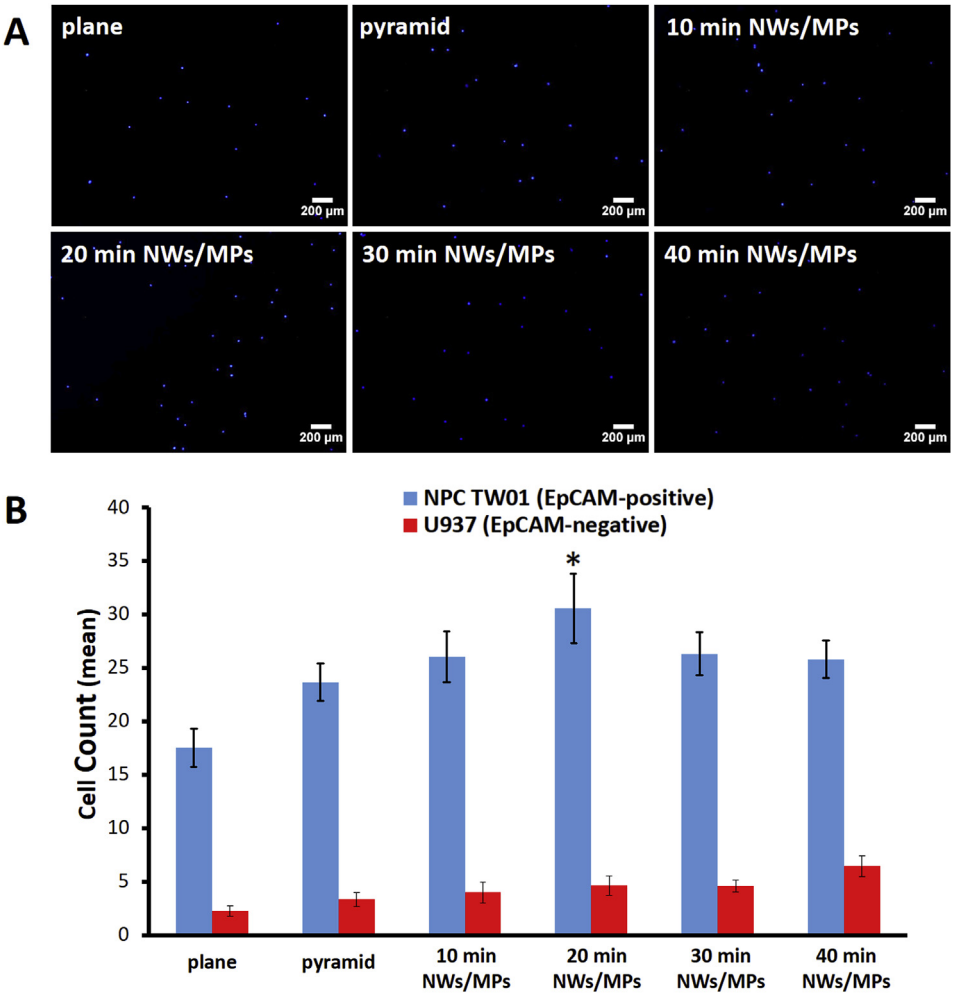

Fig. 3. (A) Cell-capture efficiency of different substrates. To test the cell-capture performance of various substrates, cell suspensions of EpCAM-positive NPC cells were introduced onto various substrate for 1 h. Captured cells were stained with DAPI. (Scale bar: 200 μM) **(B) Graph of CTCs count of NPC TW01 and U937 on different substrates.** U937 cell was used as negative control. The 20 min-etched NWs/MPs showed the best cell-capture performance. (*$p < 0.05$).

4. Discussion

4.1. CTCs

CTCs, are cancer cells shed from the primary tumor which circulate in the bloodstream, creating opportunities for metastatic spread. CTCs were first reported by Asworth in 1869 (Ashworth, 1869). Upon shedding from the primary tumor, these cells flow to other sites in the body, and about 0.01% of them lead to clinically significant metastases (Barradas and Terstappen, 2013; Fidler and Radinsky, 1990). According to previous studies, up to 90% of patients die from metastasis to distant sites rather than from the primary tumor (Weiss, 2000). Thus, the presence of CTCs is highly related to disease progression and has been shown to be correlated with prognosis in several cancers, including breast cancer (Rack et al., 2014), lung cancer (Alama et al., 2014; Chen and Xu, 2014), gastric cancer (Zheng et al., 2017), colorectal cancer (Negin and Cohen, 2010), head and neck cancers (Kulasinghe et al., 2015), especially NPC (He et al., 2017; Si et al., 2016; Wu et al., 2017), and many other malignancies. It has also been proposed that tumor burden affects the level of released CTCs, and an increase in tumor burden might increase the number of CTCs (Chen et al., 2018). In addition, CTC counts has also been proposed to be a valuable tool in assessing efficacy of treatments (Vojtechova et al., 2016).

Not only CTC count, but also specific genetic or phenotypic biomarkers on CTCs, was found to have clinical significance for cancer patients. However, there are limited studies regarding biomarker expression for CTCs. According to Li et al., the expression of post-therapeutic COX-2 in CTCs of NPC patients is an indicator of poor prognosis (Li et al., 2018). Another study regarding colorectal cancer also assessed the importance of COX-2 expression in CTCs. They found that COX-2 expression in mesenchymal CTCs correlates with the occurrence of metastasis (Cai et al., 2019). The catalytic subunit of telomerase (hTERT) was found to be higher in NPC patients and the quantity of this molecule strongly correlated with the tumor progression (Fu et al., 2017). It has been proposed that detecting multiple biomarkers on CTCs may be a promising prognosticator for patients' treatment outcome and survival in the future (Li et al., 2018). For instance, Court et al. demonstrated that detecting not all CTCs but VIM (vimentin, a mesenchymal marker)-positive CTCs may be more valuable when evaluating metastasis and determining treatments in hepatocellular carcinoma (Court et al., 2018).

4.2. NPC and CTCs

Although CTCs comprise an active area of cancer research, a paucity of data exists for applications to NPC. Wu et al. found that the decrease of CTCs in patients with locally advanced NPC is related to improved treatment outcomes. Moreover, the number of tetraploidic CTCs before treatment was found to be significant predictor (Wu et al., 2017). Chen et al. recently found that CTCs were closely associated with advanced

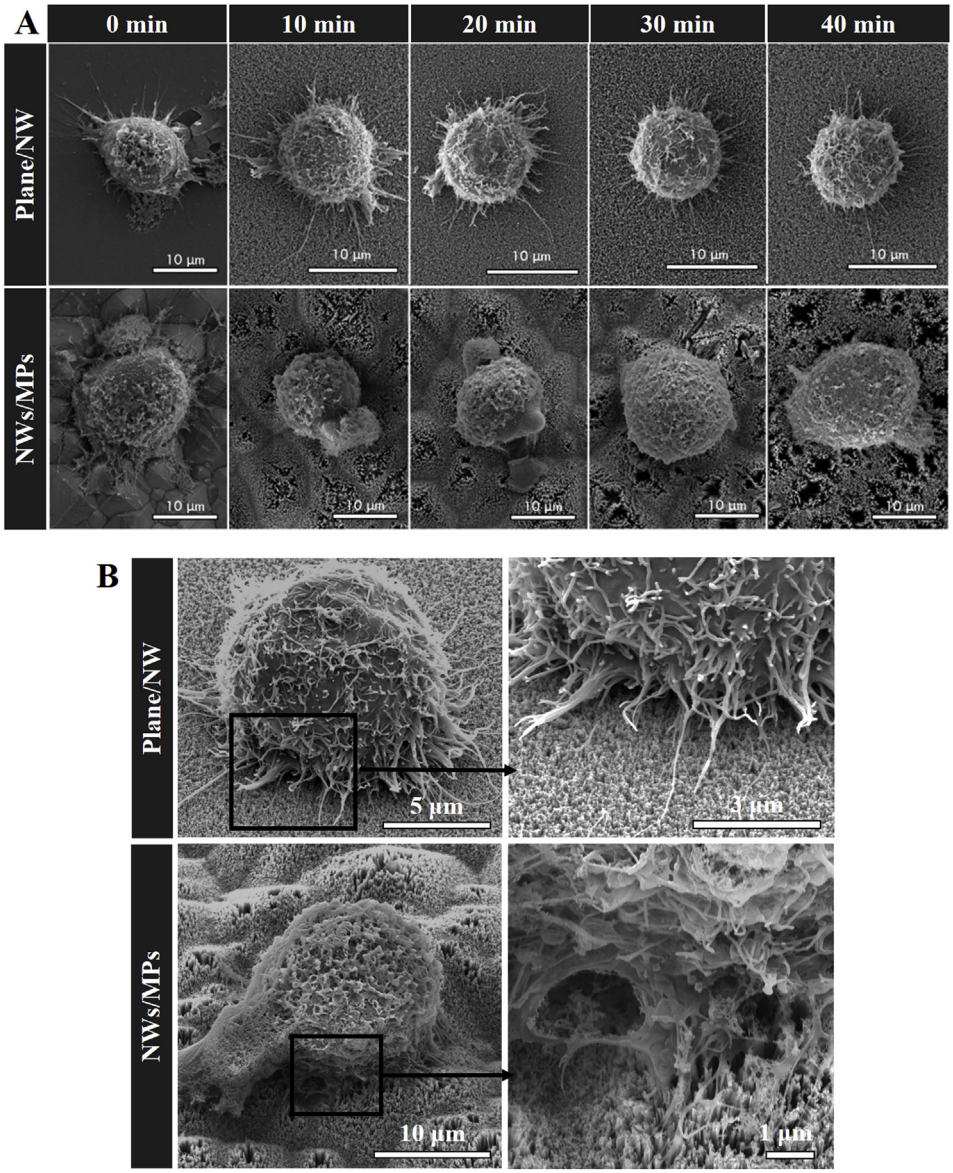

Fig. 4. (A) SEM images of CTCs on different substrates. Both lamellipodia and filopodia could be observed on the edge of the NPC cells on various substrates. Compared to CTCs on plane substrates, CTCs on Si NWs/MPs appears to have wider surface areas of spread which promote cell contact with the substrate, leading to relatively more lamellipodia being observed. **(B) SEM tilt view of CTCs on plane NWs and NWs/MPs substrates.** The filopodia of CTCs on Si NWs/MPs extends vertically down into the gaps between the NWs. (Scale bar: 10 μM).

NPC stage, and also found that advanced stage was associated with higher CTC-positive rates. They further analyzed treatment outcomes and concluded that treatment with inductive chemotherapy plus intensity-modulated radiation therapy and adjuvant chemotherapy might be more effective for CTC-positive patients with advanced NPC stages (Chen et al., 2018). He et al. differentiated NPC cells from normal blood cells by immunohistochemical staining using CK5/6 (cytokeratin 5/6), P63 markers and in situ hybridization using EBV-specific biomarker of EBV-encoded RNAs (EBERs) (He et al., 2017). Though the presence of CTCs was confirmed in NPC patients, there have been controversial results regarding the correlation between CTCs and clinical stage (Chen et al., 2018; He et al., 2017; Li et al., 2016; Wu et al., 2017). This may be due to different CTC detection methods. Therefore, refinement of current CTC detection techniques is necessary, which may not only help to guide NPC treatment, but also improve prognostication.

4.3. Various CTC capturing methods

Due to the potential clinical value of detecting the presence of CTCs and measuring CTC count, various technologies have been designed to detect CTCs. However, this has been technically challenging because there are only a few to hundreds of CTCs per 1 billion blood cells (Hou et al., 2013; Zhang et al., 2012a). CTC capturing methods can mainly be divided into two categories: biophysical and biochemical methods. There are several biophysical methods, such as separation based on cell density (Gertler et al., 2003), cell size (Hosokawa et al., 2010; Zheng et al., 2007) and label-free microfluidic chips (Tan et al., 2010). ISET method is another biophysical technique. The advantage of ISET is that the captured CTCs are viable and may permit subsequent morphological, immunocytologic, and genetic studies (Vona et al., 2000). Biochemical methods includes antibody-based methods on nanostructured substrates or immunomagnetic beads (Bai et al., 2014; Meng et al., 2015). However, low CTC-capture yield and purity are major limitations for the clinical application of bead-based approaches.

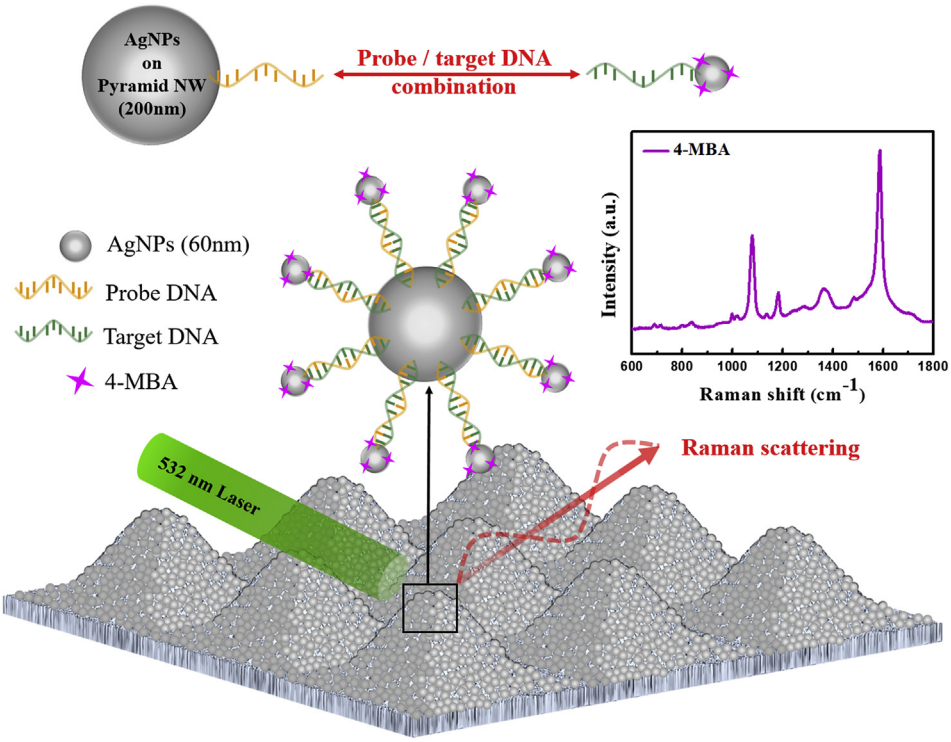

Fig. 5. Schematic illustration of EBV DNA captured on AgNPs-coated NWs/MPs and detected by Raman spectroscopy.

Both biophysical and biochemical methods have unique disadvantages. Biophysical methods may have a higher probability of false-positive or false-negative results due to individual differences of CTCs (Meng et al., 2015), while the heterogeneity of CTCs is a major problem for biochemical methods (Wang et al., 2013). CTC profiles differ in different cancers and even within the same patient. To circumvent these problems, biomarkers like EpCAM, a transmembrane glycoprotein, which are absent from hematologic cells but are commonly overexpressed in various solid tumors, are the most widely used markers for CTCs (Magbanua and Park, 2017; Yahyazadeh Mashhadi et al., 2019). There are two commercial methods for CTCs detection, including CellSearch (Veridex LLC, Raritan, New Jersey), which is FDA-approved, and the AdnaTest System (AdnaGen AG, Langenhagen, Germany). EpCAM(+) CTCs have been found to be associated with decreased progression-free survival and decreased overall survival in patients with metastatic breast, colorectal, or prostate cancer (Yahyazadeh Mashhadi et al., 2019). However, some studies revealed that the epithelial-mesenchymal transition (EMT) of CTCs may reduce the expression of epithelial protein, reducing the efficiency of the testing method utilizing EpCAM antibodies to capture CTCs. Therefore, some studies use vimentin (mesenchymal cell origin marker) to identify CTCs in NPC (Li et al., 2018). According to Chen et al., no cytokeratin (CK)18(+) CTCs were found in their NPC patients and they defined CTC positivity as CTCs $\geq$ 3 per 7.5 ml (Chen et al., 2018). Although the expression level of the EpCAM on CTCs may decrease during the EMT process, the clinical relevance of EpCAM-negative CTCs and true nature of the EMT-status of CTCs are still under investigation (Magbanua and Park, 2017).

Recently, Hoe et al. also found that advanced stage NPC specimens had higher expression of EpCAM (Hoe et al., 2017). Wang et al. showed high EpCAM expression in NPC was associated with distant metastasis and poor survival, and found that EpCAM expression in NPC cells promoted EMT (Wang et al., 2018). Therefore, we chose EpCAM as the biomarker in our CTC study. As there is currently no ideal specific cell surface marker for NPC cells, we designed our platform to have dual-function, which can isolate NPC CTCs and also can detect EBV DNA, a highly specific blood marker for NPC.

Combining elements from different isolation methods may solve the current problem (Wang et al., 2013). For example, the integration of antibody-based methods on nanostructured substrates and microfluidic chips may help to achieve more reliable CTCs separation. The advantage of label-free microfluidic chip is its high contact frequency between cells and substrates. However, the captured cells can still be easily detached from the substrate due to shearing forces. Antibody-coated nanostructured substrates introduced into microfluidic chips may have the great potential for CTC capturing in the future. The nanostructured substrates can effectively increase the surface area for capture and also increase the number of antibodies bound, both of which may enhance cell adhesion. The heterogeneity of CTCs can be readily circumvented by adding different biomarkers on different sites of each microfluidic chip (Meng et al., 2015). In recent years, several three-dimensional (3D) nanostructured substrates have been used to capture CTCs, including nanoparticles (Sekine et al., 2011), NWs (Lee et al., 2012), nanofibers (Zha et al., 2012), and nanotubes (Zhong et al., 2010). These 3D nanostructured substrates all have high surface area which could bind more capturing reagents, such as anti-EpCAM antibodies, on the substrate surface, therefore increasing the interaction and the contact frequency between CTCs and nanostructured substrates. Several CTC detection platforms based on these principles are currently being developed, with a focus on metastatic breast, colorectal, and prostate cancers. For instance, a recent study made use of AuNPs/Acetylene black (AuNPs/AB) nanomaterials to increase the detection surface area and had shown a promising result (Tang et al., 2018).

4.4. Our CTCs capturing platform – Si NWs/MPs substrates

According to Li et al. (2015), nanowire-nanostructured substrates appear to have better CTC capture efficiency than nanofibers. Therefore, we selected nanowires as the nanostructured substrate. There were already some groups using 3D-nanostructured substrates composed of Si NWs to capture CTCs in recent years since Si is usually available as electronic-grade, high-quality, and high-purity single crystalline

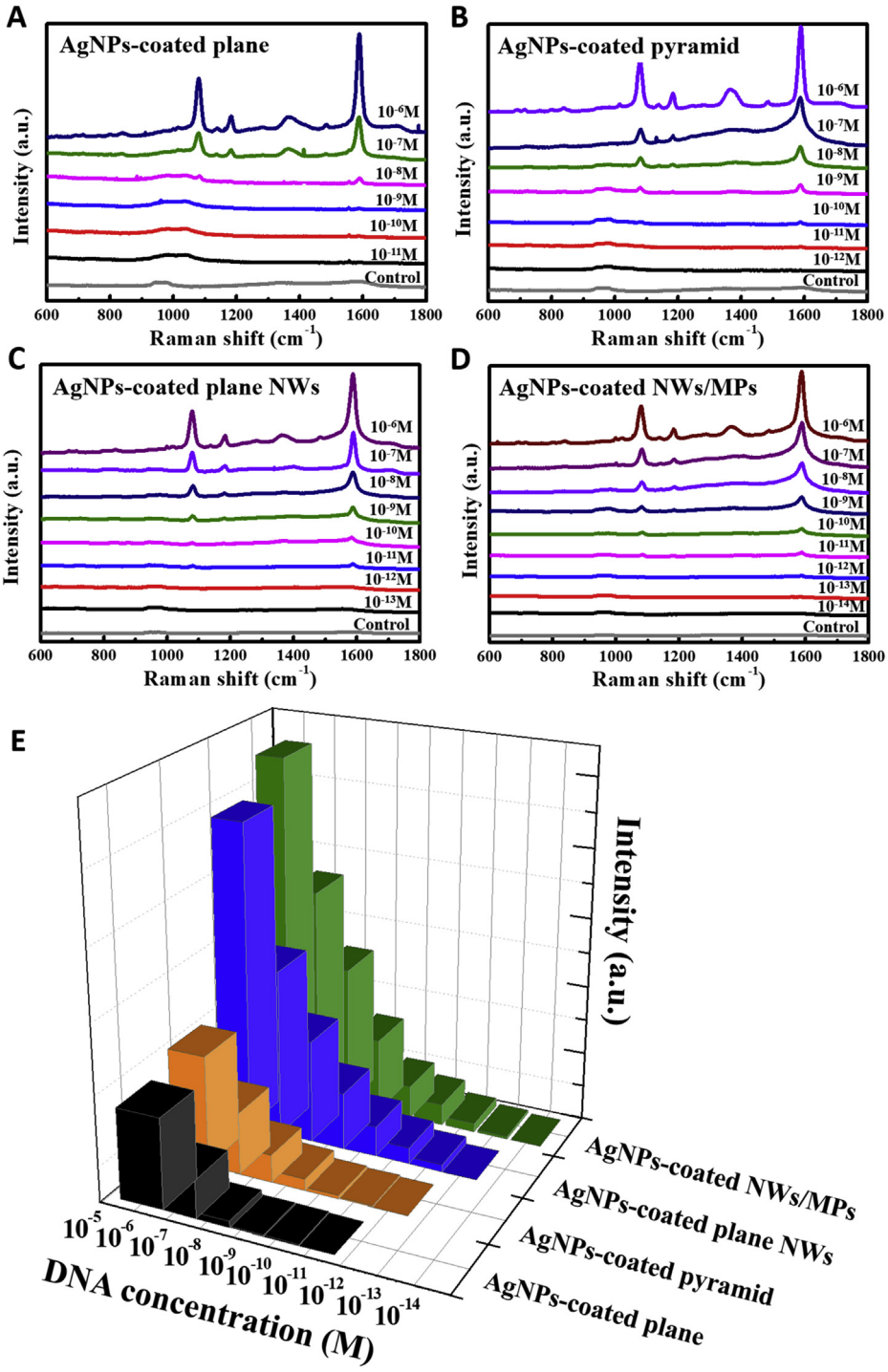

Fig. 6. (A, B, C, D)Raman results of EBV DNA detection by various AgNPs-coated substrates. Different concentration of EBV DNA was added to various AgNPs-coated substrates and SERS was used to detect the amount of EBV DNA captured. Signals at 1078 and 1596 cm^{-1} indicate hybridization of target EBV DNA and probe DNA. **(B) 3D histogram of Raman results of EBV DNA detection by various AgNPs-coated substrates.** The AgNPs-coated NWs/MPs substrate captured the greatest amount of EBV DNA, followed by the AgNPs-coated plane NWs, AgNPs-coated pyramid, and AgNPs-coated plane substrates.

material in the form of wafers. Si prevailed because it has superior physical and technological properties compared to other semiconductor materials. It is also abundant in the earth crust as an ore in the form of quartzite. With its low cost and ease of effective extraction and purification, Si is an ideal choice for biomedical applications. Mature processing technologies to fabricate functionalized, delicate, and fine structures on the wafer are also available. Wang et al. (Man et al., 2011) was the first group to employ Si NWs as a CTC capturing substrate. They (Wang et al., 2013) have successfully integrated Si NWs coated with anti-EpCAM antibody into microfluidic chips. Capture efficiency improved from about 50% to 95%, proving that Si NWs are ideal nanostructures for capturing CTCs. One of their results showed that captured yield of EpCAM-positive cells increased with increasing nanowire length (4 μm, 6 μm, 8 μm, 10 μm, and 20 μm, respectively), but the captured numbers of EpCAM-negative cells reached a maximum when the wire length was 6 μm. In our study, we further improved the surface area by integrating the NWs onto the pyramid structures. The designed uneven topography of the pyramid may not only lower the rolling

velocity of CTCs, but increase the contact points between the cells and substrate. The Si NWs/MPs substrate could be easily upscaled and prepared with low cost and has been used in solar cells to minimize light reflection and maximize surface area (Chen et al., 2015; Lee et al., 2013). Until now, however, there are no studies applying Si NWs/MPs to capturing CTCs.

Here we chemically designed and fabricated the Si NWs/MPs substrates with different NW length and also compared the efficiency to capture CTCs between plane substrate, NWs, MPs, and NWs/MPs with different Si NW lengths. Our results indicated that the cell-capture yield of Si NWs/MPs substrate was significantly higher than that using the plane substrate, reflecting enhanced cell-capture yields by using 3D nanostructures. In addition, NW modification enables CTCs to interact with the substrate more efficiently, providing higher sensitivity among all experiment groups. In our study, Si NWs/MPs with different NW length were fabricated by altering etching times (10, 20, 30, 40 min). Interestingly, the optimal parameter is at 20 min but not 40 min, which is contrary to the findings by Wang et al. This may be attributed to the uneven topography of MPs on the substrates, which sustain the bottom side of CTCs and prevent it from shear stress, having a greater chance to immobilize CTCs on the substrate. Both 30- and 40-min etched substrates have a longer wire length, but with the increase of etching time, the pyramid structures would be flattened. The 20-min-etched substrate has a better capture yield than that of the 10-min-etched one, because the 20-min-etched substrate has longer wire length and maintains the pyramid morphology. Thus, not only nanowire length, but also surface topography, can enhance capture efficiency. For comparison, EpCAM-negative (U937) cell was employed as a control (Supplementary Fig. 1). The mean counts were much lower than for NPC cells and only little differences were found between different substrates, showing that the pyramid NW substrate coated with anti-EpCAM antibody is specific for capturing EpCAM-positive cells with high sensitivity (Fig. 3). We further stained the captured cells by immunofluorescence and demonstrated that the captured NPC cells were positive for EpCAM, vimentin, CK 8 + 18, while negative for CD45 (Supplementary Fig. 2). Furthermore, the platform demonstrated good cell capture efficiency, with good sensitivity and specificity (Supplementary Fig. 3).

4.5. Cell adhesion of Si NWs/MPs substrates

Cell adhesion is also a very important factor for CTC capture. There are many studies focusing on local topographic interactions between various nanostructured substrates and cells (Dang and Leong, 2007; Liu and Chen, 2007; Yang et al., 2007), including how the nanostructures affect cellular behavior (Dang and Leong, 2007; Liu and Chen, 2007; Yang et al., 2007), such as morphology (Dalby et al., 2007; Kandere-Grzybowska et al., 2005; Park et al., 2007b), viability (Chen et al., 1997; Park et al., 2007a), adhesion (Chang et al., 2005; Park et al., 2007b; Sun et al., 2007), migration (Jiang et al., 2005; Yim et al., 2005; Yousaf et al., 2001), and differentiation (Dalby et al., 2007; Dang and Leong, 2007; Wang et al., 2009). The cytoskeleton beneath the cell surface can help to immobilize captured cells on the substrates. It is postulated that 3D nanostructure, such as the Si NWs/MPs substrates, enhances local topographic interactions with lamellipodia and filopodia on the cellular surface, which likely account for its high cell-capture affinity when compared to unstructured plane substrates (Wang et al., 2009). To confirm this, we used SEM to investigate captured CTCs on different substrates. The SEM images are shown in Fig. 4. The cell spread area of CTCs on Si NWs/MPs appears to be greater than the cell spread area of the CTCs on plane NWs. Likely as a result of this, lamellipodia are more often observed on the edges of NPC CTCs on Si NWs/MPs (Fig. 4). The filopodia of CTCs on Si NWs/MPs also extends vertically down into the gaps between the NWs. All of the above mechanical characteristics may improve cell adhesion and may be the key to the higher sensitivity of the NWs/MPs substrate to capture CTCs.

4.6. Quantitative detection of EBV DNA by AgNPs-coated NWs/MPs

The quantitative level of circulating EBV DNA has been documented to be a proxy parameter for tumor volume in NPC patients. It is found to be correlated with NPC stage and prognosis (Lo, 2001). Plasma levels of EBV DNA has been proposed to be a superior prognostic tool than traditional EBV VCA antibodies, and has been found to be highly correlated to disease status of NPC patients (Lin et al., 2004; Lo et al., 2000; Twu et al., 2007). EBV DNA is typically measured by real-time quantitative polymerase chain reaction (PCR). He et al. used the ISET method as well as in situ hybridization of EBERs (EBV-encoded RNAs) to capture CTCs in NPC patients and found a positive correlation between CTC counts and EBV DNA (He et al., 2017). The uniqueness of our platform is the 3D novel Si NWs/MPs hybrid nanostructure, which not only can specifically isolate NPC CTCs with high CTC-capture efficiency, but also can be used for detecting EBV DNA. In our study, we demonstrated that AgNPs-coated NWs/MPs substrate was the best to capture EBV DNA, followed by the AgNPs-coated plane NW, pyramid, and plane substrates (Fig. 6). Higher EBV DNA concentration led to higher laser scattering intensity, indicating higher amount of captured EBV DNA.

SERS is a vibrational spectroscopic technique which has recently emerged as an ultrasensitive, versatile, and powerful detection tool for liquid biopsy analysis, such as CTCs, exosomes, circulating tumor DNAs, microRNAs and cancer-related proteins (Chen et al., 2019; Ferhan et al., 2018; Zhang et al., 2019). The advantages of SERS include high sensitivity and specificity, minimal sample consumption and manipulation, time efficiency, and multiplexing capabilities. Additionally, SERS offers intrinsic vibrational fingerprint spectra of biomolecules, which helps to identify individual components within the complex biological milieu (Chen et al., 2019; Zhang et al., 2019). Compared to traditional fluorescence spectroscopy, SERS needs only a single laser to excite all SERS labels, and can detect different targets simultaneously due to its narrow peak width (~1–2 nm, about 10–100 times narrower than fluorescence emission bands). Moreover, SERS tags possesses higher photostability, which avoids interference by autofluorescence from bio-samples and photobleaching (Tsoutsi et al., 2018; Zong et al., 2018). As an ultrasensitive tool for analysis of bioactive molecules, SERS possesses great potential to be translated into clinical use not only for disease diagnosis and also treatment monitoring.

Regarding electrical sensing of DNA, various technologies have been developed with high sensitivity, such as electrochemical impedance, electrochemiluminescence, and field-effect transistor sensors. However, most of these modalities are designed for detection of a specific target DNA only. In contrast, the current dual-function platform can isolate CTCs as well as detect DNA. Furthermore, electrical DNA biosensors are not able to detect multiple targets simultaneously like SERS (Abbott et al., 2017; Hu et al., 2019).

Both CTCs and EBV DNA are good biomarkers for NPC, providing prognostic and predictive value. This dual-function nanostructured platform is able to isolate NPC CTCs, but may also detect EBV DNA at very low concentrations. The platform possesses potential valuable clinical applications, such as early detection and monitoring cancer progression and surveillance of therapeutic efficacy in NPC patients. Moreover, it may pave the way for finding novel treatment modalities to minimize metastasis-associated NPC morbidity and mortality. Only a small amount of blood (probably 1 cc) may be enough for sampling. The next generation of the platform will be designed to improve capture sensitivity and specificity by integration multiple cancer-specific antibodies immobilized on the surfaces, such as EpCAM, vimentin, cytokeratin 8/18, and CD44. Further clinical studies will be conducted soon to validate this technology in a practical setting. We believe our platform has the potential to become a promising tool for clinical applications in NPC disease monitoring and treatment outcome assessment in the near future.

5. Conclusion

In this study, the Si NWs/MPs platform based on 3D nanostructured substrates demonstrated efficient cell capture ability, and can, at the same time, sensitively detect EBV DNA at very low concentrations. Further clinical validation is needed to elucidate to true translational value of this technology. It is conceivable that this platform has great potential to become a promising diagnostic tool for monitoring disease status and predicting prognosis of NPC patients in the near future.

Conflicts of interest

All the authors declare that they have no conflict of interest.

Acknowledgements

This research was supported by grants from the Taipei Veterans General Hospital (V107B-009), and Ministry of Science and Technology (MOST106-2314-B-075 -035 -MY3) to MYL. The authors thank Clinical Research Core Laboratory at Taipei Veterans General Hospital for the facility support.

Appendix A. Supplementary data

Supplementary data to this article can be found online at https://doi.org/10.1016/j.bios.2019.111509

References

Abbott, J., Ham, D., Xu, G., 2017. Methods Mol. Biol. 1572, 169–187.
Alama, A., Truini, A., Coco, S., Genova, C., Grossi, F., 2014. Drug Discov. Today 19, 1671–1676.
Ashworth, T., 1869. Australas. Med. J. 14, 146.
Attard, G., Swennenhuis, J.F., Olmos, D., Reid, A.H., Vickers, E., A'Hern, R., Levink, R., Coumans, F., Moreira, J., Riisnaes, R., Oommen, N.B., Hawche, G., Jameson, C., Thompson, E., Sipkema, R., Carden, C.P., Parker, C., Dearnaley, D., Kaye, S.B., Cooper, C.S., Molina, A., Cox, M.E., Terstappen, L.W., de Bono, J.S., 2009. Cancer Res. 69, 2912–2918.
Bai, L., Du, Y., Peng, J., Liu, Y., Wang, Y., Yang, Y., Wang, C., 2014. J. Mater. Chem. B 2, 4080–4088.
Barradas, A.M., Terstappen, L.W., 2013. Cancers (Basel) 5, 1619–1642.
Bruce, J.P., Yip, K., Bratman, S.V., Ito, E., Liu, F.F., 2015. J. Clin. Oncol. 33, 3346–3355.
Cai, J., Huang, L., Huang, J., Kang, L., Lin, H., Huang, P., Zhu, P., Wang, J., Dong, J., Wang, L., Xian, C.J., 2019. J. Cell. Biochem. 120, 4935–4941.
Chang, W.C., Lee, L.P., Liepmann, D., 2005. Lab Chip 5, 64–73.
Chen, C., Liu, W., Tian, S., Hong, T., 2019. Sensors (Basel) 19.
Chen, C.S., Mrksich, M., Huang, S., Whitesides, G.M., Ingber, D.E., 1997. Science 276, 1425–1428.
Chen, H.Y., Lu, H.L., Ren, Q.H., Zhang, Y., Yang, X.F., Ding, S.J., Zhang, D.W., 2015. Nanoscale 7, 15142–15148.
Chen, Y.Y., Xu, G.B., 2014. Med. Oncol. 31, 240.
Chen, Z., Xu, L., Xu, X., Yuan, C., 2018. Oncol. Lett. 15, 6283–6290.
Chua, M.L.K., Wee, J.T.S., Hui, E.P., Chan, A.T.C., 2016. Lancet 387, 1012–1024.
Cohen, S.J., Punt, C.J., Iannotti, N., Saidman, B.H., Sabbath, K.D., Gabrail, N.Y., Picus, J., Morse, M., Mitchell, E., Miller, M.C., Doyle, G.V., Tissing, H., Terstappen, L.W., Meropol, N.J., 2008. J. Clin. Oncol. 26, 3213–3221.
Court, C.M., Hou, S., Winograd, P., Segel, N.H., Li, Q.W., Zhu, Y., Sadeghi, S., Finn, R.S., Ganapathy, E., Song, M., French, S.W., Naini, B.V., Sho, S., Kaldas, F.M., Busuttil, R.W., Tomlinson, J.S., Tseng, H.R., Agopian, V.G., 2018. Liver Transplant. 24, 946–960.
Dalby, M.J., Gadegaard, N., Tare, R., Andar, A., Riehle, M.O., Herzyk, P., Wilkinson, C.D., Oreffo, R.O., 2007. Nat. Mater. 6, 997–1003.
Dang, J.M., Leong, K.W., 2007. Adv. Mater. 19, 2775–2779.
Danila, D.C., Fleisher, M., Scher, H.I., 2011. Clin. Cancer Res. 17, 3903–3912.
Doyen, J., Alix-Panabieres, C., Hofman, P., Parks, S.K., Chamorey, E., Naman, H., Hannoun-Levi, J.M., 2012. Crit. Rev. Oncol. Hematol. 81, 241–256.
Farace, F., Massard, C., Vimond, N., Drusch, F., Jacques, N., Billiot, F., Laplanche, A., Chauchereau, A., Lacroix, L., Planchard, D., Le Moulec, S., Andre, F., Fizazi, K., Soria, J.C., Vielh, P., 2011. Br. J. Canc. 105, 847–853.
Ferhan, A.R., Jackman, J.A., Park, J.H., Cho, N.J., Kim, D.H., 2018. Adv. Drug Deliv. Rev. 125, 48–77.
Fidler, I.J., 2003. Nat. Rev. Cancer 3, 453–458.
Fidler, I.J., Radinsky, R., 1990. J. Natl. Cancer Inst. 82, 166–168.
Fu, X., Shen, C., Wang, H., Chen, F., Li, G., Wen, Z., 2017. BMC Canc. 17, 479.
Gertler, R., Rosenberg, R., Fuehrer, K., Dahm, M., Nekarda, H., Siewert, J.R., 2003. Recent Results Cancer Res. 162, 149–155.
He, C., Huang, X., Su, X., Tang, T., Zhang, X., Ma, J., Guo, X., Lv, X., 2017. Cancer Biol. Ther. 18, 888–894.
Hoe, S.L.L., Tan, L.P., Abdul Aziz, N., Liew, K., Teow, S.Y., Abdul Razak, F.R., Chin, Y.M., Mohamed Shahrehan, N.A., Chu, T.L., Mohd Kornain, N.K., Peh, S.C., Koay, C.E., Lo, K.W., Ahmad, M., Ng, C.C., Khoo, A.S., 2017. Sci. Rep. 7, 12372.
Hosokawa, M., Hayata, T., Fukuda, Y., Arakaki, A., Yoshino, T., Tanaka, T., Matsunaga, T., 2010. Anal. Chem. 82, 6629–6635.
Hou, S., Zhao, H., Zhao, L., Shen, Q., Wei, K.S., Suh, D.Y., Nakao, A., Garcia, M.A., Song, M., Lee, T., Xiong, B., Luo, S.C., Tseng, H.R., Yu, H.H., 2013. Adv. Mater. 25, 1547–1551.
Hu, Z., Suo, Z., Liu, W., Zhao, B., Xing, F., Zhang, Y., Feng, L., 2019. Biosens. Bioelectron. 131, 237–249.
Jiang, X., Bruzewicz, D.A., Wong, A.P., Piel, M., Whitesides, G.M., 2005. Proc. Natl. Acad. Sci. U.S.A. 102, 975–978.
Kandere-Grzybowska, K., Campbell, C., Komarova, Y., Grzybowski, B.A., Borisy, G.G., 2005. Nat. Methods 2, 739–741.
Krebs, M.G., Sloane, R., Priest, L., Lancashire, L., Hou, J.M., Greystoke, A., Ward, T.H., Ferraldeschi, R., Hughes, A., Clack, G., Ranson, M., Dive, C., Blackhall, F.H., 2011. J. Clin. Oncol. 29, 1556–1563.
Kulasinghe, A., Perry, C., Jovanovic, L., Nelson, C., Punyadeera, C., 2015. Int. J. Cancer 136, 2515–2523.
Lee, I.-J., Paik, U., Park, J.-G., 2013. Sol. Energy 91, 256–262.
Lee, S.K., Kim, G.S., Wu, Y., Kim, D.J., Lu, Y., Kwak, M., Han, L., Hyung, J.H., Seol, J.K., Sander, C., Gonzalez, A., Li, J., Fan, R., 2012. Nano Lett. 12, 2697–2704.
Li, F., Liu, J., Song, D., Zhang, Q., Ding, N., He, X., 2016. Acta Otolaryngol. 136, 1164–1167.
Li, Y.J., Luo, Y., Xie, X.Q., Li, P., Wang, F., 2018. Radiother. Oncol. 129, 396–402.
Li, Y.Q., Chandran, B.K., Lim, C.T., Chen, X., 2015. Adv Sci (Weinh) 2, 1500118.
Lin, C.T., Chan, W.Y., Chen, W., Huang, H.M., Wu, H.C., Hsu, M.M., Chuang, S.M., Wang, C.C., 1993. Lab. Investig. 68, 716–727.
Lin, C.T., Wong, C.I., Chan, W.Y., Tzung, K.W., Ho, J.K., Hsu, M.M., Chuang, S.M., 1990. Lab. Investig. 62, 713–724.
Lin, J.C., Wang, W.Y., Chen, K.Y., Wei, Y.H., Liang, W.M., Jan, J.S., Jiang, R.S., 2004. N. Engl. J. Med. 350, 2461–2470.
Lin, T.W., Wu, H.Y., Tasi, T.T., Lai, Y.H., Shen, H.H., 2015. Phys. Chem. Chem. Phys. 17, 18443–18448.
Liu, W.F., Chen, C.S., 2007. Adv. Drug Deliv. Rev. 59, 1319–1328.
Lo, Y.M., 2001. Ann. N. Y. Acad. Sci. 945, 68–72.
Lo, Y.M., Chan, A.T., Chan, L.Y., Leung, S.F., Lam, C.W., Huang, D.P., Johnson, P.J., 2000. Cancer Res. 60, 6878–6881.
Magbanua, M.J.M., Park, J.W., 2017. Isolation and Molecular Characterization of Circulating Tumor Cells. Springer.
Man, Y., Wang, Q., Kemmner, W., 2011. J. Clin. Exp. Pathol. 1 2161-0681.1000102.
Meng, J., Liu, H., Wang, S., 2015. Nanostructured substrates for circulating tumor cell capturing. In: Chen, X., Fuchs, H. (Eds.), Soft Matter Nanotechnology: from Structure to Function, first ed. ed. John Wiley & Sons, pp. 293–308.
Miller, M.C., Doyle, G.V., Terstappen, L.W., 2010. J. Oncol. 2010, 617421.
Negin, B.P., Cohen, S.J., 2010. Curr. Treat. Options Oncol. 11, 1–13.
Park, J., Bauer, S., von der Mark, K., Schmuki, P., 2007a. Nano Lett. 7, 1686–1691.
Park, S.Y., Park, S.Y., Namgung, S., Kim, B., Im, J., Kim, J.Y., Sun, K., Lee, K.B., Nam, J.M., Park, Y., 2007b. Adv. Mater. 19, 2530–2534.
Paterlini-Brechot, P., Benali, N.L., 2007. Cancer Lett. 253, 180–204.
Petersson, F., 2015. Semin. Diagn. Pathol. 32, 54–73.
Rack, B., Schindlbeck, C., Juckstock, J., Andergassen, U., Hepp, P., Zwingers, T., Friedl, T.W., Lorenz, R., Tesch, H., Fasching, P.A., Fehm, T., Schneeweiss, A., Lichtenegger, W., Beckmann, M.W., Friese, K., Pantel, K., Janni, W., 2014. J. Natl. Cancer Inst. 106.
Schlange, T., Pantel, K., 2016. Pharmacogenomics 17, 183–186.
Sekine, J., Luo, S.C., Wang, S., Zhu, B., Tseng, H.R., Yu, H.H., 2011. Adv. Mater. 23, 4788–4792.
Si, Y., Lan, G., Deng, Z., Wang, Y., Lu, Y., Qin, Y., Huang, B., Yang, Y., Weng, J., Han, X., Zhang, B., Qin, Y., Xiong, W., Li, B., Wu, S., 2016. Jpn. J. Clin. Oncol. 46, 622–630.
Sun, T., Han, D., Riehemann, K., Chi, L., Fuchs, H., 2007. J. Am. Chem. Soc. 129, 1496–1497.
Swaby, R.F., Cristofanilli, M., 2011. BMC Med. 9, 43.
Tan, S.J., Lakshmi, R.L., Chen, P., Lim, W.T., Yobas, L., Lim, C.T., 2010. Biosens. Bioelectron. 26, 1701–1705.
Tang, S., Shen, H., Hao, Y., Huang, Z., Tao, Y., Peng, Y., Guo, Y., Xie, G., Feng, W., 2018. Biosens. Bioelectron. 104, 72–78.
Tsoutsi, D., Sanles-Sobrido, M., Cabot, A., Gil, P.R., 2018. Curr. Med. Chem. 25, 4638–4652.
Twu, C.W., Wang, W.Y., Liang, W.M., Jan, J.S., Jiang, R.S., Chao, J., Jin, Y.T., Lin, J.C., 2007. Int. J. Radiat. Oncol. Biol. Phys. 67, 130–137.
Vojtechova, G., Benesova, L., Belsanova, B., Minarikova, P., Levy, M., Lipska, L., Suchanek, S., Zavoral, M., Minarik, M., 2016. Advances in Clinical and Experimental Medicine, vol. 25. official organ Wroclaw Medical University, pp. 1273–1279.
Vona, G., Sabile, A., Louha, M., Sitruk, V., Romana, S., Schutze, K., Capron, F., Franco, D., Pazzagli, M., Vekemans, M., Lacour, B., Brechot, C., Paterlini-Brechot, P., 2000. Am. J. Pathol. 156, 57–63.
Wang, L., Asghar, W., Demirci, U., Wan, Y., 2013. Nano Today 8, 347–387.
Wang, M.H., Sun, R., Zhou, X.M., Zhang, M.Y., Lu, J.B., Yang, Y., Zeng, L.S., Yang, X.Z., Shi, L., Xiao, R.W., Wang, H.Y., Mai, S.J., 2018. Cell Death Dis. 9, 2.
Wang, S., Wang, H., Jiao, J., Chen, K.J., Owens, G.E., Kamei, K., Sun, J., Sherman, D.J., Behrenbruch, C.P., Wu, H., Tseng, H.R., 2009. Angew. Chem., Int. Ed. Engl. 48, 8970–8973.
Weiss, L., 2000. Cancer Metastasis Rev. 19 (I-xi), 193–383.
Wu, Y., Qian, Y., Peng, J., Wei, X., Yuan, Z., Zhou, F., Hu, D., 2017. J. Clin. Oncol. 35, e17523.

Yahyazadeh Mashhadi, S.M., Kazemimanesh, M., Arashkia, A., Azadmanesh, K., Meshkat, Z., Golichenari, B., Sahebkar, A., 2019. J. Cell. Physiol. 234, 12569–12580.
Yang, M.T., Sniadecki, N.J., Chen, C.S., 2007. Adv. Mater. 19, 3119–3123.
Yim, E.K., Reano, R.M., Pang, S.W., Yee, A.F., Chen, C.S., Leong, K.W., 2005. Biomaterials 26, 5405–5413.
Yousaf, M.N., Houseman, B.T., Mrksich, M., 2001. Angew. Chem., Int. Ed. Engl. 40, 1093–1096.
Zeng, Y.-J., Lee, S.-W., Lan, M.-Y., 2017. J. Nanosci. Nanotechnol. 17, 9095–9100.
Zha, Z., Jiang, L., Dai, Z., Wu, X., 2012. Appl. Phys. Lett. 101, 193701.
Zhang, N., Deng, Y., Tai, Q., Cheng, B., Zhao, L., Shen, Q., He, R., Hong, L., Liu, W., Guo, S., Liu, K., Tseng, H.R., Xiong, B., Zhao, X.Z., 2012a. Adv. Mater. 24, 2756–2760.
Zhang, X., Servos, M.R., Liu, J., 2012b. Chem. Commun. 48, 10114–10116.
Zhang, Y., Mi, X., Tan, X., Xiang, R., 2019. Theranostics 9, 491–525.
Zhe, X., Cher, M.L., Bonfil, R.D., 2011. Am. J. Cancer Res. 1, 740–751.
Zheng, S., Lin, H., Liu, J.Q., Balic, M., Datar, R., Cote, R.J., Tai, Y.C., 2007. J. Chromatogr. A 1162, 154–161.
Zheng, X., Fan, L., Zhou, P., Ma, H., Huang, S., Yu, D., Zhao, L., Yang, S., Liu, J., Huang, A., Cai, C., Dai, X., Zhang, T., 2017. Transl. Oncol. 10, 431–441.
Zhong, X., Bai, H.J., Xu, J.J., Chen, H.Y., Zhu, Y.H., 2010. Adv. Funct. Mater. 20, 992–999.
Zong, C., Xu, M., Xu, L.J., Wei, T., Ma, X., Zheng, X.S., Hu, R., Ren, B., 2018. Chem. Rev. 118, 4946–4980.